Deprotonation of Isoxazole: A Photoelectron Imaging Study

Adam A. Wallace, Yerbolat Dauletyarov, Andrei Sanov*

Department of Chemistry and Biochemistry, The University of Arizona, Tucson, Arizona 85721, United States

ABSTRACT. We report a photoelectron imaging study of gas-phase deprotonation of isoxazole, in which spectroscopic data are compared to the results of electronic structure calculations for the anion products corresponding to each of three possible deprotonation sites. The observed photoelectron spectra are assigned to a mixture of the anion isomers. Deprotonation at the most acidic (C5), as well as the least acidic (C4) positions yields the respective C5- and C4-isoxazolide anions, while the reaction at the intermediate-acidity C3 site leads to a cleavage of the O−N bond and an opening of the ring in the anion. Following photodetachment, the ground states of neutral C5- and C4-isoxazolyl are assigned to be σ radicals (X^2A′), while the ground-state neutral derived from the ring-open C3-anion is a π radical (X^2A″). The relative intensities of the spectral bands exhibit sensitivity to the ion source conditions, giving evidence of competing and varying contributions of the dominant C5 and C3, as well as possible C4, deprotonation pathways.

1. Introduction

Isoxazole is heterocyclic molecule, an isomer of oxazole. The two structures are shown in the following scheme:

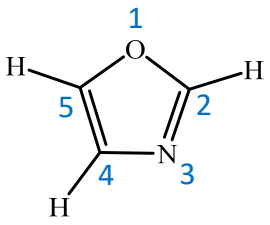

Oxazole

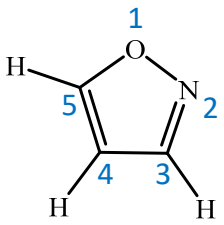

Isoxazole

(Scheme 1)

The difference between the oxazole and isoxazole structures is the change in location of the nitrogen atom from the third position within the heterocyclic ring in oxazole to the second position, next to the oxygen atom, in isoxazole. One of the goals of this study is to investigate the chemical effect of this change.

Isoxazole, known for its straightforward synthesis, is often used as scaffolding for therapeutic agents.[1] Its other wide-ranging applications span organic synthesis, pharmaceuticals, and pesticides.[2-3] However, many important aspects of its chemistry remain unexplored, especially in regard to the radical and negative-ion derivatives. Past studies of isoxazole mostly focused on the closed-shell neutral molecule shown in Scheme 1 and the corresponding cation.[4-7] In the present work, we focus on the closed-shell anions obtained via the deprotonation of isoxazole, as well as the corresponding monovalent neutral radicals accessed in the photodetachment of the anions. These highly reactive species may play crucial roles in the variety of reaction pathways. Using a combination of experimental and theoretical techniques, we investigate their molecular and electronic structures and determine the respective anion detachment energies and neutral radical electron affinities. These properties are viewed in comparison to the analog oxazole molecule.[8]

There are three possible deprotonation sites in either oxazole or isoxazole. Following the conventional numbering system defined in Scheme 1, the possible deprotonation sites in oxazole are C2, C4, and C5, compared to C3, C4, and C5 in isoxazole. Each site potentially yields a distinct isomer of the respective oxazolide or isoxazolide anion. Based on the electronegativities of the neighboring atoms (increasing from C to N to O), one expects the acidity—and hence the ease of deprotonation—to decrease from C2 to C5 to C4 in oxazole and from C5 to C3 to C4 in isoxazole. These predictions are consistent with the past studies. Specifically, under the gas-phase plasma conditions similar to the experiments described here, oxazole was shown to deprotonate selectively at the most acidic C2 position,[8] while collision-induced dissociation experiments by Adams *et al.* showed preferred deprotonation of isoxazole at C5 and C3.[9] Cole *et al.* attempted to selectively deprotonate isoxazole at C5 via collisional decarboxylation of isoxazole-5-carboxylic acid, but found that upon collision isoxazole lost HCN rather than the carboxy group.[10] Computational work by Kaur *et al.* confirmed that the C5 site in isoxazole is more acidic than C4, while deprotonation at C3 led to the breaking of the O–N bond, making the C3 comparison more challenging.[11] In a study of 1H-1,2,3-triazole, a 5-member heterocyclic aromatic with three nitrogen atoms, Ichino *et al.* found that deprotonation at various carbon positions initiated fragmentation or N-N bond fission.[12]

In the present study, we explore the deprotonation of isoxazole in its gas-phase reaction with O^- and the various anion states that result. These include the C5- and C4-isoxazolide anions and the ring-open anion species resulting from isoxazole deprotonation at the C3 position. The relative energetics of the anion isomers, as well as the corresponding neutral radicals, are examined using a combination of photoelectron spectroscopy and theoretical methods.

2. Experimental Methods

The experiments were performed using the negative-ion photoelectron imaging spectrometer described in detail elsewhere,[13] with certain changes introduced to the ion generation process, as described below. The anions were obtained by expanding a neutral isoxazole precursor seeded in O_2 or N_2O gas through a pulsed supersonic nozzle (General Valve, Inc., Series 9), operated at a repetition rate of either 20 or 50 Hz, to match that of the laser. The precursor isoxazole vapor was picked up from the liquid sample (99%; Sigma Aldrich, Inc.) kept at ambient room temperature, while the carrier gas was passed over the liquid at a backing pressure of approximately 2.5 atm. The 52 torr vapor pressure of isoxazole at 25°C resulted in a 2.5-3% mixture of the precursor and the carrier gas.

The supersonic expansion was intersected by electrons from a thoria-coated iridium filament (e-Filaments, LLC) floated at ~300V, generating negative ions via a slow secondary electron attachment mechanism. In this work, the filament was placed 3 cm downstream from the nozzle and 1.5 cm away from the expansion axis. In the experiments with oxygen as a carrier gas, a 5×5 cm^2 stainless steel plate, kept at the same potential as the filament, was placed on the side of the expansion opposite the filament. The addition of the plate minimized the field deflection of the generated ions and allowed the experiments to be run with a lower current through the filament, extending its useful life. Hereafter, these ion generation conditions will be referred to as ion source A. In contrast, the conditions using the N_2O carrier gas, without the metal plate opposing the electron filament, will be referred to as source B.

The atomic oxygen anions, formed in the resulting plasma from either O_2 or N_2O, were presumed to react with isoxazole, resulting in its deprotonation.[14] The anions were then separated according to their masses in a time-of-flight mass spectrometer and interrogated by ~7 ns duration 355, 306,

or 266 nm laser pulses. The 355 and 266 nm light was produced as the third and fourth harmonics, respectively, of a Nd:YAG laser (Spectra Physics, Inc., model Lab-130). The 306 nm light was obtained by frequency doubling the 612 nm output of a Nd:YAG pumped dye laser (ND6000, Continuum, Inc.) operating on Rhodamine 640 dye.

The electrons photodetached[15] from the mass-selected anions were projected using a velocity-map[16] imaging[17-18] (VMI) assembly onto a 40 mm diameter position-sensitive dual microchannel plate detector located 18 cm away from the laser interaction region, in the direction perpendicular to both the ion and laser beams. The detector is coupled to a P43 phosphor screen and the resulting photoelectron images are recorded using a charge-coupled device camera (Photometrics, Inc., CoolSnap Myo). All images reported here correspond to multiple experimental runs totaling ~10^6 experimental cycles each. The results were analyzed via an inverse Abel transformation[18] using the BASEX program.[19]

3. Experimental Results

The raw photoelectron images of deprotonated isoxazole, collected using ion source A at 266 nm, 306 nm, and 355 nm are presented in Figure 1(a)-(c), alongside the corresponding spectra. All photoelectron spectra in this work are plotted versus electron binding energy, eBE = $h\nu$ – eKE, where $h\nu$ is the photon energy and eKE is the electron kinetic energy. Unlike the seemingly similar case of oxazolide, studied by our group previously,[8] no clear vibrational resolution was achieved in this work, with one exception discussed in Section 5. The lack of resolved vibrational progressions is due to the naturally congested spectra and overlapping contributions of more than one anion isomer. The experimental resolution itself is similar to the previous work.

All three spectra in Figure 1 exhibit a dominant photodetachment transition at ~3 eV. It is usually assumed that the position of a photodetachment band maximum corresponds to the vertical

detachment energy (VDE). However, based on the analysis in Sections 4 and 5, this dominant band is attributed to a mixture of anion isomers; hence the maximum position does not necessarily correspond to the VDE of any particular anion.

The 355 nm spectrum in Figure 1(a) shows a low-eBE shoulder for the dominant spectral band. This shoulder is also discernable, albeit not as clearly, in the 306 and 266 nm spectra in Figures 1(b) and (c), respectively. The intensity of the shoulder was observed to change significantly depending on the ion generation conditions. This behavior is consistent with the presence of more than one anion isomer, whose relative populations vary depending on the ion source conditions. To emphasize this point, Figure 2(a) and (b) compares the 355 nm spectra of the ions generated using ion sources A and B, respectively. The low-eBE shoulder in Figure 2(b) is not only enhanced in relative intensity, compared to Figure 2(a), but also shows a partially resolved vibrational progression with an average spacing of 0.11(1) eV or 890(80) cm^{-1}.

As can be seen by visual inspection of the data in Figure 1, the photoelectron images exhibit slightly perpendicular photoelectron angular distributions (PADs). The values of the photoelectron anisotropy parameter β corresponding to different photodetachment bands are indicated next to them in the photoelectron spectra. The β values were determined by analyzing the angular dependence of the images, integrated in the energy domain over the full width at half-maximum of the corresponding spectral peaks.[19-20] Compared to other heterocyclic aromatics,[21] little variation of β for different transitions or as a function of eKE is observed in this work. We attribute this, in part, to the spectral overlap of different anion isomers, as discussed in the following Sections.

4. Theoretical Modeling

As discussed in the Introduction, the ease of deprotonation in isoxazole is expected to decrease from C5 to C3 to C4 (Scheme 1). Past studies showed deprotonation at C5 and C3,[9] and consistent

with these observations, the sensitivity of the photoelectron spectra to the ion source conditions in the present work suggests the existence of more than one active deprotonation site, resulting in competing reaction pathways and products. No such sensitivity was noted in the previous work on oxazolide, where only one anion isomer was observed.[8]

To assist in the interpretation of the results, we carried out geometry optimizations and selected potential energy scans for the deprotonated isoxazole anions, as well as the corresponding neutral radicals. The calculations were performed using the QChem software package.[22] The coupled-cluster theory with single and double excitations (CCSD) was used for all anion geometry optimizations. The anion VDEs and neutral electron affinities (EA) were calculated using the equation-of-motion (EOM) ionization-potential (IP) formalism, combined with the coupled-cluster theory.[23] For each stable isomer of the anion, the VDEs were determined for transitions to two lowest electronic states of the corresponding neutral radical: the $^2A'$ (σ-radical) and $^2A''$ (π-radical) states. The respective VDE(σ) and VDE(π) values were obtained from single-point EOM-IP-CCSD calculations for optimized anion structures, removing the highest-energy appropriate-symmetry electron from the closed-shell anion reference.

Attempts to optimize the neutral structures at the CCSD level of theory using unrestricted Hartree-Fock orbitals resulted in significant spin contamination: $\langle S^2 \rangle \approx 1.1$, compared to the expected 0.75. This approach was therefore deemed unreliable. Instead, the geometries of the ground and first excited electronic states of the neutral radicals were optimized using the unrestricted EOM-IP-CCSD method. The advantage of this approach is the use of a closed-shell (anion) reference, which does not suffer from spin contamination. Each neutral state was accessed by removing an appropriate-symmetry electron from the robust anion reference, and the geometry was optimized by following the potential gradient of the target state. The adiabatic electron

affinities or adiabatic electron attachment/binding energies were calculated as energy differences between the respective geometry-optimized neutral and anion states. For brevity, both the electron affinities (for the ground states) and the adiabatic attachment energies (for the excited states) are hereafter referred to as electron affinities of the corresponding states. All CCSD and EOM-IP-CCSD calculations reported here employed the aug-cc-pVTZ basis set. Where noted, additional quick surveying calculations and potential energy scans were performed using the B3LYP density functional with the aug-cc-pVDZ basis set.

The results of the calculations are summarized in Figure 3, which shows the anion structures and their relative energetics, with the three panels corresponding to isoxazole deprotonation at the C5, C3, and C4 positions, in the order of decreasing acidity. The C5, C3, and C4 panels are labeled in green, blue, and red; these colors are also used in Figures 1 and 2 to color-code the spectral assignments and model spectra. The complete geometric parameters of the optimized anion and ground-state neutral structures are presented in Table S1 in Supplemental Information. Vibrational frequency calculations were used to verify that the anion structures shown correspond to true potential minima.

As expected, the calculations show that C4 deprotonation is less favorable than C5, by 0.30 eV. This value was determined by comparing the CCSD energies of the optimized C5- and C4-isoxazolide structures. It is impossible to give a corresponding value for isoxazole deprotonation at the C3 position, because this process triggers the dissociation of the N–O bond, followed by the opening of the ring. Relaxed potential energy scans (B3LYP/aug-cc-pVDZ) with respect to the C4–C3–N bond angle in C3-isoxazolide showed no barrier to the ring opening, contrasting the C5 and C4 deprotonation pathways, both of which keep the ring intact. Since the immediate product of C3 deprotonation, C3-isoxazolide, is not a stationary structure, it does not possess an energy

eigenvalue. This is indicated schematically by a shaded energy band representing C3-isoxazolide in Figure 3.

As shown at the bottom of Figure 3, the opening of the ring in C3-isoxazolide does produce an equilibrium anion structure, whose IUPAC name is (Z)-2-cyanoethen-1-olate. We will refer to it, for brevity, as C3-enolate, where the prefix indicates its origin from C3 deprotonation of isoxazole. There is no information in the literature about previous studies of this anion. Allowing fleeting liberty with the nomenclature in referring to C3-enolate as the *cis* (with respect to the C4=C5 bond) isomer, it should be noted that the corresponding *trans* form, (E)-2-cyanoethen-1-olate (not shown), is 0.095 eV (B3LYP/aug-cc-pVDZ) more stable than the *cis* structure shown. However, a potential energy scan with respect to the C4=C5 torsion angle (B3LYP/aug-cc-pVDZ) indicates a 1.3 eV barrier separating the *cis* and *trans* anions, consistent with the π bonding character included in the C4=C5 bond. Therefore, we deem the *trans*-C3-enolate anion to be inaccessible in the present experiments and make no further reference to it here.

As seen in Figure 3, the ring opening from C3-isoxazolide to C3-enolate results in significant stabilization of the anion. According to CCSD/aug-cc-pVTZ, C3-enolate is 2.82 eV more stable than C5-isoxazolide. However, the final-state energetics should not be taken to indicate that the C3 species must dominate the anion population. The formation of all anion isomers involves an initial deprotonation step, which is followed by a downhill ring-opening in the C3 case only. Since little coupling can be conceived between the final C3, C4, and C5 structures, their relative populations are determined by the relative ease of the initial C3 vs. C4 vs. C5 deprotonation steps. Since the acidity considerations indicate that C5 deprotonation is slightly more favorable (initially) than C3, the formation of C5-isoxazolide may be more efficient than the formation of the (ultimately) more stable C3-enolate form. Considering the energetics of an electron-impact ionized plasma,

even the C4 deprotonation in our experiment cannot be ruled out *a priori*.

The neutral state energies are also indicated in Figure 3 based on the EOM-IP-CCSD results. For each anion isomer, the two lowest neutral electronic states are described: one corresponding to the σ radical (^{2}A′ state) and one to the π radical (^{2}A″ state). In Figure 3, each radical state is represented by two energy levels: one (shown by solid horizontal lines) is obtained via a vertical detachment transition from the relaxed anion structure and the other (dashed horizontal lines) corresponds to a relaxed neutral geometry. For each neutral state, the energy difference between the "solid" level and the optimized anion structure corresponds to the anion VDE, while the difference between the "dashed" level and the optimized anion structure is the neutral's EA. The difference between the "solid" and "dashed" neutral energy levels, i.e. (VDE – EA), is the neutral state's relaxation energy.

The ring-closed C4- and C5-isoxazolide anions, as well as the ring-open C3-enolate, are closed-shell ^{1}A′ species. The completely filled HOMO and HOMO−1 orbitals of each of the anion isomers are shown in Figure 4. The ground states of neutral C5- and C4-isoxazolyl correspond to σ radicals (X^2A′) formed by electron ejection from the *a′* HOMO of the respective anions. As expected, these HOMOs have significant C5/C4 (respectively) sp^2 hybrid character. The corresponding canonical orbital of the C5/C4-isoxazolyl radical would combine with the 1*s* orbital of H to form the C5/C4-H σ bond in isoxazole molecule. The first excited states of C5- and C4-isoxazolyl are π radicals (A^2A″) formed by electron ejection from the *a″* HOMO−1 of the corresponding anions.

The HOMO and HOMO-1 of ring-closed C3-isoxazolide (not shown) are similar to their C4 and C5 counterparts in that they too are σ (*a′*) and π (*a″*) in their respective characters, with the HOMO having a large contribution from the C3 sp^2 hybrid. However, the ordering of these orbitals changes upon the opening of the ring, with the π orbital becoming the HOMO of the C3-enolate anion. The

immediate implication of this change is that the lowest-energy photodetachment transition in C3-enolate accesses the π-radical ground state of the neutral, while the σ-radical becomes an excited state, as seen in Figure 3. The σ-character HOMO−1 of C3-enolate (Figure 4) includes no sp^2 hybrid contribution from the deprotonated carbon, C3. In fact, the C3 atom in C3-enolate is in the *sp* hybridization state. Instead, the *a′* HOMO−1 includes dominant contributions from the C5 (not C3) sp^2 hybrids, coupled with the in-plane *p* orbital on the oxygen atom. Overall, this HOMO−1 has, predominantly, a clear *d*-like character, qualitatively similar to the π_g^* HOMO of O_2^-.

As seen in Figure 3, the relaxation energies, VDE − EA, of the σ radical states are consistently larger than those of the π radicals for each of the three isomers. This is to be expected, because the removal of an electron from an in-plane MO results in a greater distortion of the molecular geometry compared to the removal of an electron from an out-of-plane MO. We further note that the slightly negative anisotropy values reported in Figure 1 are consistent with the detachment from all types of orbitals illustrated in Figure 4. Past studies and analysis using the *s-p* mixed character model predicted moderately negative β values in the detachment from in-plane σ orbitals of similar heterocyclics with significant sp^2 hybrid character.[21,24] Similarly, negative values of the anisotropy parameter should be expected based on qualitative symmetry considerations in the detachment form π type MOs,[25] as well as from *d*-like MOs,[24,26-28] similar to C3-enolate's *a′* HOMO−1. Hence, in the deprotonation of isoxazole, we have relatively small expected anisotropy variation for different photodetachment transitions, combined with the co-existence of different anion isomers with partially overlapping photoelectron spectra. It is not surprising, therefore, that little quantitative analysis of the PADs could be carried out in this work, beyond the general qualitative conclusion about the agreement of the experimental observations with the model predictions.

5. Discussion

The experimental images and spectra in this work are assigned to a combination of the anion isomers resulting from the deprotonation of the precursor isoxazole molecule. The past studies[9] provided evidence of isoxazole deprotonation at C5 and C3 positions, but not at C4. The ion-generation conditions in our experiment are drastically different and the excitation energies existing within the electron-impact ionized plasma in our ion source may be sufficient to activate deprotonation even at the most unfavorable C4 position. This contrasts the behavior of oxazole (where deprotonation was observed at only one position),[8] but since these are chemically distinct molecules there is no reason to expect their deprotonation behaviors to be similar.

The past oxazole work relied on definitive mass-spectrometric data for the deuterated form of the compound to draw the conclusion about its selective deprotonation.[8] Similarly, concrete experimental evidence would be needed to rule out any deprotonation pathways in isoxazole. The available evidence does not provide sufficient basis for excluding any of the pathways. To the contrary, the observed changes in the spectra depending on the ion source conditions point to an opposite conclusion: that there are indeed multiple active deprotonation pathways in isoxazole within the electron-impact-ionized plasma.

To facilitate the spectral assignments, the VDE and EA values from Figure 3 are also indicated in Figure 1, using specifically designed triangular graphs superimposed with the experimental spectra. The graphs follow the isomer color scheme adopted throughout: green for the anion resulting from C5 deprotonation of isoxazole, blue for C3, and red for C4. Two triangular graphs are shown for each isomer in Figures 1(b) and (c): one for each of the two lowest photodetachment transitions, accessing the σ and π radical states, for a total of six transitions. In Figure 1(a), two of the higher-energy transitions are not shown, because they fall too far outside the photon energy

range. The key to the energetic triangles is given in Figure 1(d). For example, the σ(5) label corresponds to the $X\,^1\mathrm{A}' \rightarrow X\,^2\mathrm{A}'$ transition in C5-isoxazolide, producing the C5-isoxazolyl σ-radical. The bold vertical sides of the triangles should be viewed as traditional stick-spectra, indicating the VDEs of the transitions. The position of the left vertex of each triangle indicates the adiabatic electron affinity of the corresponding neutral state. The length of the horizontal side, corresponding to the difference between the VDE and the EA is, therefore, the relaxation energy of the neutral radical. The relaxation energy serves as an indication of the expected width of the Franck-Condon envelope of the corresponding transition. In comparing the experimental spectra in Figure 1 to the spectrum of the calculated triangles, one should keep in mind that the EOM-IP-CCSD calculations achieve better accuracy in describing the lowest-energy photodetachment transitions, compared to the excited states. Finally, while we cannot predict either the relative isomer populations or the corresponding photodetachment cross-sections, we do expect, on energetic grounds, the contribution of the C4 anion isomer to be smaller than that of either C5 or C3. This expectation is indicated by the reduced height of the C4 triangles in Figure 1.

Comparing the experimental and theoretical results in Figure 1, we conclude that none of the three possible anion isomers can be definitively excluded from consideration. As discussed above, the coexistence of the C5 and C3 isomers is expected, based on the past results,[9] deprotonation energetics, and the observed dependence of the spectra on the ion source conditions in this work. However, even the highest-energy C4 isomer cannot be excluded based on the available data. In particular, the long low-eBE shoulder of the main photodetachment band appears consistent with σ photodetachment of a combination of the C5 and C4 isoxazolide isomers, i.e. transitions σ(5) and σ(4). The more pronounced band peaking at about 3 eV is attributed to the lowest-energy transition in C3-enolate, π(3). The broader right shoulder of the dominant peak in the 306 and 266

nm spectra is attributed to the second transition in C5-isoxazolide, π(5). This shoulder is most pronounced at 266 nm and least visible at 355 nm, consistent with the near-threshold Wigner suppression of the electronic part of the photodetachment cross-section.[29-30] The separate band, appearing at higher energies in the 306 and 266 nm spectra and peaking at eBE > 4 eV in the latter, is assigned to the second transition in C3-enolate, σ(3), but the π(4) transition may also be contributing to the lower-eBE shoulder of this band.

To examine the competition of the anion isomers, we modelled the 355 nm photoelectron spectra obtained using different ion-source conditions. The results are in Figure 2. As seen by comparing the experimental spectra in (a) and (b), the low-eBE shoulder in the source-A spectrum is smaller, relative to the dominant peak, compared to the similar shoulder in the source-B spectrum. These spectral variations are consistent with the existence of competing deprotonation pathways in the parent isoxazole molecule, yielding coexisting anion isomers with varying relative populations.

In modeling these spectra, we rolled the C5 and C4 contributions into a single band and modeled the spectra as superpositions of two Wigner-scaled Gaussians (WSG): one, WSG(4/5), corresponding to C5- and C4-isoxazolide and one, WSG(3)—to C3-enolate. A WSG is a normalized Gaussian function of eBE, multiplied by an $eKE^{1/2} = (h\nu - eBE)^{1/2}$ pre-factor. The Gaussians simulate the Franck-Condon envelopes of the transitions, with the maximum positions corresponding to the VDE, while the pre-factor accounts for the near-threshold scaling of the electronic cross-sections. The form of the scaling function corresponds to the Wigner law,[29] with the orbital angular momentum quantum number of the outgoing free electron $l = 0$. Granted, the final state in the observed transitions is a superposition of partial waves with different l values. However, in the low-eKE regime, where the Wigner scaling is most important, the *s* waves dominate (assuming they are allowed by the selection rules). In the absence of detailed information about the partial-

wave composition, the above scaling function is most appropriate, if only approximate. This approach to modeling of photoelectron spectra has been previously tested on other systems.[31-32]

In each case shown in Figures 2(a) and (b), a superposition of WSG(4/5) and WSG(3) model functions was matched to the experimental spectra. The expansion coefficients, Gaussian positions (VDEs) and widths were treated as adjustable parameters. In each case, the two WSG components of the spectral simulation are shown in the figure, superimposed with the experimental spectrum. The lower-eBE function, WSG(4/5), corresponds to VDE = 2.85 eV, which is the calculated VDE(σ) value for C5-isoxazolide (Figure 3). The contribution of C4 is expected to be smaller and important at the lower-eBE edge of the shoulder, accounting for its calculated VDE(σ) = 2.60 eV). The second function, WSG(3), describes the π-radical transition in C3-enolate and corresponds to a VDE of 3.01 eV, to be compared to VDE(π) = 3.08 eV calculated for this isomer. Based on these spectral simulations, we recommend the 2.85(5) eV and 3.01(2) eV values for the VDEs of C5-isoxazolide and C3-enolate, respectively.

In both Figures 2(a) and (b) the Gaussian part of WSG(3) is narrower than that of WSG(4/5). This is consistent with not only the existence of two anion isomers potentially ascribed to the latter, but also the smaller neutral relaxation energy associated with the π(3) transition compared to both σ(4) and σ(5), as seen in Figure 3. Turning to the relative weights of the different isomers, without knowing the relative magnitudes of the photodetachment cross-sections, it is impossible to determine the relative isomer populations from the spectra. However, the fractional population of C3-enolate is clearly greater in ion source A compared to B.

Using the relative amplitudes of WSG(3) and WSG(4/5) model functions from Figures 2(a) and (b), it is possible to partially deconvolute the source A and source B experimental spectra into the individual contributions of the anion isomers. This is shown in Figure 2(c) for ion source B.

Because we have two independent data sets (sources A and B), the deconvolution yields, accordingly, two independent component spectra. One, shown in Figure 2(c) in blue, corresponds to the $\pi(3)$ transition in C3-enolate. The other, shown using a combination of red and green colors, corresponds to the $\sigma(4/5)$ transitions in C4- and C5-isoxazolide. Armed with the knowledge that the C4 isomer contributes at the lower-eBE tail of the band, we roughly divide the overall C4/C5 spectrum into the individual red (C4) and green (C5) parts. The stitching point at eBE ≈ 2.5 eV is chosen approximately, on the account of EA = 2.46 eV calculated for the C5 isomer.

Near the peak of the WSG(4/5) model function, the experimental spectrum in Figure 2(b) reveals a faint signature of a vibrational progression attributed to C5-isoxazolide. This progression is less discernable in Figure 2(a), because the C5 spectrum there is overwhelmed by the larger contribution of C3-enolate. The 0.11(1) eV or 890(80) cm^{-1} spacing between the vibrational peaks agrees well with the 892 cm^{-1} frequency of an in-plane ring-distortion mode in C5-isoxazolyl, predicted based on the B3LYP/aug-cc-pVDZ harmonic frequency calculation. It also agrees well with the same-frequency, 890(80) cm^{-1}, vibrational progression observed in the photoelectron spectrum of C2-oxazolide, assigned to a similar in-plane ring-distortion mode in the oxazolyl radical.[8]

Finally, we comment that the VDE of C5-isoxazolide, 2.85(5) eV, is sizably larger than the corresponding value for C2-oxazolide, 2.66(2) eV. A similar difference applies to the adiabatic EAs of the corresponding isoxazolyl and oxazolyl radicals. Although the EA of isoxazolyl could not be determined reliably from the experimental data in this work, the high-level calculations place this value for the C5-radical at 2.46 eV (Figure 3), in general agreement with the experiment. This is to be compared to the experimentally determined EA of C2-oxazolyl, 2.21(2) eV.[8] Overall, a quarter-of-an-electron-volt increase in electron binding energies in deprotonated isoxazole, compared to oxazole, may explain the multiple active deprotonation pathways in isoxazole, contrasting

the sole pathway observed in oxazole.

6. Summary and Conclusions

Deprotonation of isoxazole can occur at three distinct positions. The reactions at the most acidic (C5), as well as the least acidic (C4) positions yield the respective C5- and C4-isoxazolide anions, while the deprotonation at the intermediate-acidity C3 site leads to a cleavage of the O−N bond and an opening of the ring in the anion. The photoelectron spectra of deprotonated isoxazole are assigned to a mixture of predominantly C5-isoxazolide, with a VDE of 2.85(5) eV, and C3-enolate, with a VDE of 3.01(2) eV, with a possible contribution from C4-isoxazolide. The above VDE for C5-isoxazolide is sizably larger than the VDE = 2.66(2) eV of C2-oxazolide, formed via the most acidic and the sole observed deprotonation pathway in oxazole. In contrast to oxazolide, the relative intensities of the isoxazolide spectral bands exhibit sensitivity to the ion source conditions, giving evidence of competing and varying contributions of the different deprotonation pathways. The lowest energy photodetachment transitions in the C5- and C4-isoxazolide anions access the σ-radical ($X\,^2\mathrm{A}'$) ground states of C5- and C4-isoxazolyl, respectively, while the ground-state neutral derived from ring-open C3-enolate is a π radical ($X\,^2\mathrm{A}''$).

ASSOCIATED CONTENT

Supporting Information

The Supporting Information is available free of charge on the ACS Publications website at DOI: xxxxxxx.

Table S1: Geometric parameters of the equilibrium anion and neutral structures resulting from the deprotonation or H-dissociation of isoxazole at the C5, C3, or C4 positions, calculated at the CCSD level of theory with the aug-cc-pVTZ basis set. (PDF)

AUTHOR INFORMATION

Corresponding Author

*Email: sanov@arizona.edu

ORCID

Andrei Sanov: 0000-0002-2373-4387

Author Contributions

The manuscript was written through contributions of all authors. All authors have given approval to the final version of the manuscript.

Funding Sources

U.S. National Science Foundation Grant CHE-1664732.

Notes

The authors declare no competing financial interest

ACKNOWLEDGMENT

The authors gratefully acknowledge the support of this work by the U.S. National Science Foundation through Grant CHE-1664732.

REFERENCES

1. Sysak, A.; Obminska-Mrukowicz, B., Isoxazole Ring as a Useful Scaffold in a Search for New Therapeutic Agents. *Eur. J. Med. Chem.* **2017,** *137*, 292-309.

2. Zhu, J.; Mo, J.; Lin, H. Z.; Chen, Y.; Sun, H. P., The Recent Progress of Isoxazole in Medicinal Chemistry. *Biorg. Med. Chem.* **2018,** *26*, 3065-3075.

3. Lamberth, C., Oxazole and Isoxazole Chemistry in Crop Protection. *J. Heterocycl. Chem.* **2018,** *55*, 2035-2045.

4. Kobayashi, T.; Kubota, T.; Ezumi, K.; Utsunomiya, C., Photoelectron Angular-Distribution Study of Some Isoxazoles Combined with Perturbation Theoretic Approach. *Bull. Chem. Soc. Jpn.* **1982,** *55*, 3915-3919.

5. Modelli, A.; Burrow, P. D., Electron Attachment to the Aza-Derivatives of Furan, Pyrrole, and Thiophene. *J. Phys. Chem. A* **2004,** *108*, 5721-5726.

6. Turchi, I. J.; Dewar, M. J. S., Chemistry of Oxazoles. *Chem. Rev.* **1975,** *75*, 389-437.

7. Palmer, M. H.; Findlay, R. H.; Egdell, R. G., Electronic-Structure of Heteroaromatic Molecules: Ab Initio Calculations and Photoelectron Spectra for Isomeric Oxazoles and Some Isomeric Oxadiazoles. *J. Mol. Struct.* **1977,** *40*, 191-210.

8. Culberson, L. M.; Blackstone, C. C.; Wysocki, R.; Sanov, A., Selective Deprotonation of Oxazole and Photoelectron Imaging of the Oxazolide Anion. *Phys. Chem. Chem. Phys.* **2014,** *16*, 527-532.

9. Adams, G. W.; Bowie, J. H.; Hayes, R. N., Negative-Ion Fragmentations of Deprotonated Heterocycles. The Isothiazole, Thiazole, Isoxazole, and Oxazole Ring-Systems. *Int. J. Mass Spectrom.* **1992,** *114*, 163-182.

10. Cole, C. A.; Demarais, N. J.; Yang, Z. B.; Snow, T. P.; Bierbaum, V. M., Heterocyclic Anions of Astrobiological Interest. *Astrophys. J.* **2013,** *779*, 181.

11. Kaur, D.; Khanna, S.; Kaur, R. P., The Role of Conjugative Interactions in Acidic and Basic Character of Five Membered Aromatic Heterocyclics. *J. Mol. Struct.* **2010,** *949*, 14 - 22.

12. Ichino, T.; Andrews, D. H.; Rathbone, G. J.; Misaizu, F.; Calvi, R. M. D.; Wren, S. W.; Kato, S.; Bierbaum, V. M.; Lineberger, W. C., Ion Chemistry of 1h-1,2,3-Triazole. *J. Phys. Chem. B* **2008,** *112*, 545-557.

13. Velarde, L.; Habteyes, T.; Sanov, A., Photodetachment and Photofragmentation Pathways in the $[(Co_2)_2(H_2o)_M]^-$ Cluster Anions. *J. Chem. Phys.* **2006,** *125*, 114303.

14. Lee, J.; Grabowski, J. J., Reactions of the Atomic Oxygen Radical-Anion and the Synthesis of Organic Reactive Intermediates. *Chem. Rev.* **1992,** *92*, 1611-1647.

15. Ervin, K. M.; Lineberger, W. C., Photoelectron Spectroscopy of Negative Ions. In *Advances in Gas Phase Ion Chemistry*, Adams, N. G.; Babcock, L. M., Eds. JAI Press: Greenwich, 1992; Vol. 1, pp 121-166.

16. Eppink, A. T. J. B.; Parker, D. H., Velocity Map Imaging of Ions and Electrons Using Electrostatic Lenses: Application in Photoelectron and Photofragment Ion Imaging of Molecular Oxygen. *Rev. Sci. Instrum.* **1997,** *68*, 3477-3484.

17. Chandler, D. W.; Houston, P. L., Two-Dimensional Imaging of State-Selected Photodissociation Products Detected by Multiphoton Ionization. *J. Chem. Phys.* **1987,** *87*, 1445-1447.

18. Heck, A. J. R.; Chandler, D. W., Imaging Techniques for the Study of Chemical Reaction Dynamics. *Annu. Rev. Phys. Chem.* **1995,** *46*, 335-372.

19. Dribinski, V.; Ossadtchi, A.; Mandelshtam, V. A.; Reisler, H., Reconstruction of Abel-Transformable Images: The Gaussian Basis-Set Expansion Abel Transform Method. *Rev. Sci. Instrum.* **2002,** *73*, 2634-2642.

20. Zare, R. N., Photoejection Dynamics. *Mol. Photochem.* **1972,** *4*, 1-37.

21. Culberson, L. M.; Blackstone, C. C.; Wallace, A. A.; Sanov, A., Aromatic Stabilization and Hybridization Trends in Photoelectron Imaging of Heterocyclic Radicals and Anions. *J. Phys. Chem. A* **2015,** *119*, 9770-9777.

22. Shao, Y.; Molnar, L. F.; Jung, Y.; Kussmann, J.; Ochsenfeld, C.; Brown, S. T.; Gilbert, A. T. B.; Slipchenko, L. V.; Levchenko, S. V.; O'Neill, D. P., et al., Advances in Methods and Algorithms in a Modern Quantum Chemistry Program Package. *Phys. Chem. Chem. Phys.* **2006,** *8*, 3172-3191.

23. Krylov, A. I., Equation-of-Motion Coupled-Cluster Methods for Open-Shell and Electronically Excited Species: The Hitchhiker's Guide to Fock Space. *Annu. Rev. Phys. Chem.* **2008,** *59*, 433-462.

24. Sanov, A., Laboratory-Frame Photoelectron Angular Distributions in Anion Photodetachment: Insight into Electronic Structure and Intermolecular Interactions. *Annu. Rev. Phys. Chem.* **2014,** *65*, 341-363.

25. Khuseynov, D.; Blackstone, C. C.; Culberson, L. M.; Sanov, A., Photoelectron Angular Distributions for States of Any Mixed Character: An Experiment-Friendly Model for Atomic, Molecular, and Cluster Anions. *J. Chem. Phys.* **2014,** *141*, 124312.

26. Reed, K. J.; Zimmerman, A. H.; Andersen, H. C.; Brauman, J. I., Cross Sections for Photodetachment of Electrons from Negative Ions near Threshold. *J. Chem. Phys.* **1976,** *64*, 1368-1375.

27. Akin, F. A.; Schirra, L. K.; Sanov, A., Photoelectron Imaging Study of the Effect of Monohydration on O_2^- Photodetachment. *J. Phys. Chem. A* **2006,** *110*, 8031-8036.

28. Mabbs, R.; Mbaiwa, F.; Wei, J.; Van Duzor, M.; Gibson, S. T.; Cavanagh, S. J.; Lewis, B. R., Observation of Vibration-Dependent Electron Anisotropy in O_2^- Photodetachment. *Phys. Rev. A* **2010,** *82*, 011401.

29. Wigner, E. P., On the Behavior of Cross Sections near Thresholds. *Phys. Rev.* **1948,** *73*, 1002-1009.

30. Mead, R. D.; Lykke, K. R.; Lineberger, W. C., Photodetachment Threshold Laws. In *Electronic and Atomic Collisions*, Eichler, J.; Hertel, I. V.; Stolterfoht, N., Eds. Elsevier: Amsterdam, 1984; pp 721-730.

31. Khuseynov, D.; Dixon, A. R.; Goebbert, D. J.; Sanov, A., Heterogeneous Substitution Effects in Chlorocyanomethyl Radical and Chlorocyanocarbene. *J. Phys. Chem. A* **2013,** *117*, 10681–10691.

32. Surber, E.; Sanov, A., Imaging of Direct Photodetachment and Autodetachment of $(OCS)_2^-$: Excited-State Dynamics of the Covalent Dimer Anion. *Phys. Rev. Lett.* **2003,** *90*, 093001.

Figure 1

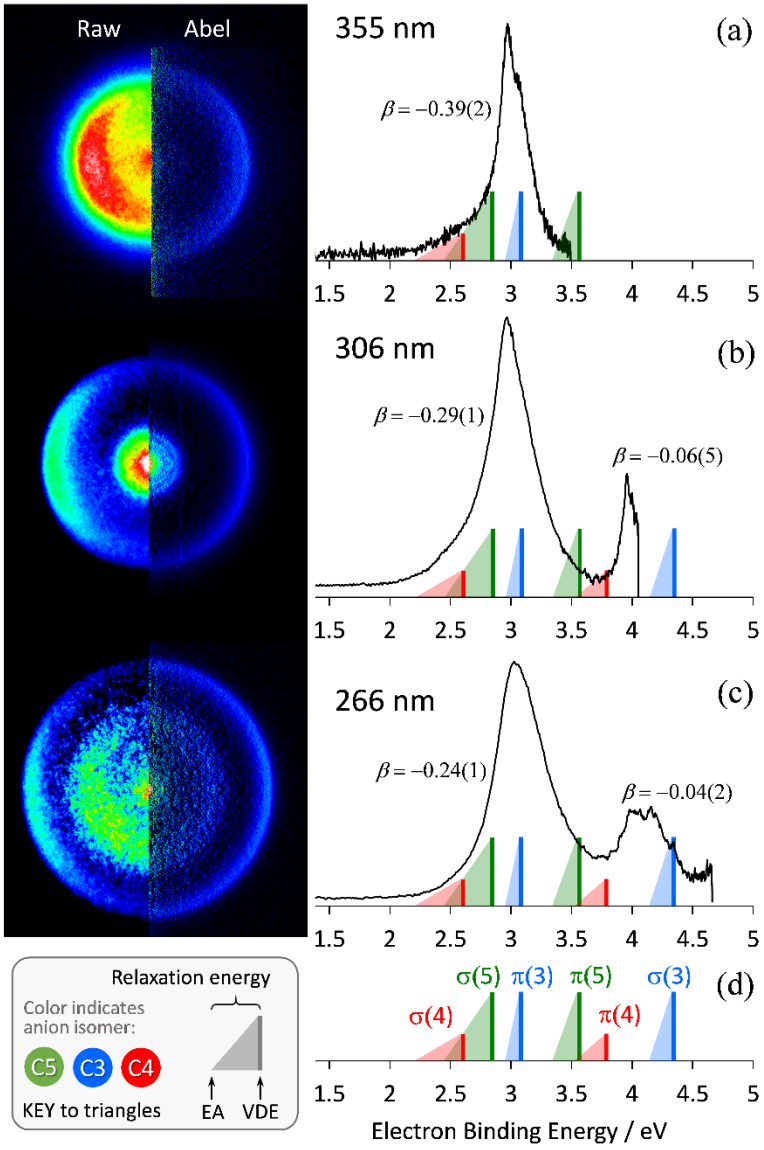

Figure 1. Composite raw and Abel-inverted photoelectron images (left and right halves, respectively) and the corresponding photoelectron spectra of deprotonated isoxazole obtained at (a) 355 nm, (b) 306 nm, and (c) 266 nm. The spectrum of triangular graphs in (d), also superimposed for

clarity and convenience with the experimental spectra in (a)-(c), summarizes the results of the EOM-IP-CCSD/aug-cc-pVTZ calculations for the C5-, C3-, and C4-anion isomers, described in Section 4. The bold vertical sides of the triangles represent the VDEs of the indicated transitions and should be viewed, collectively, as traditional stick-spectra. The left vertices of the triangles indicate the EAs of the corresponding neutral states. The lengths of the horizontal sides, therefore, correspond to the neutral-radical relaxation energies, serving as an indication of the expected width of the Franck-Condon envelope of each corresponding transition. See Section 5 for details.

Figure 2

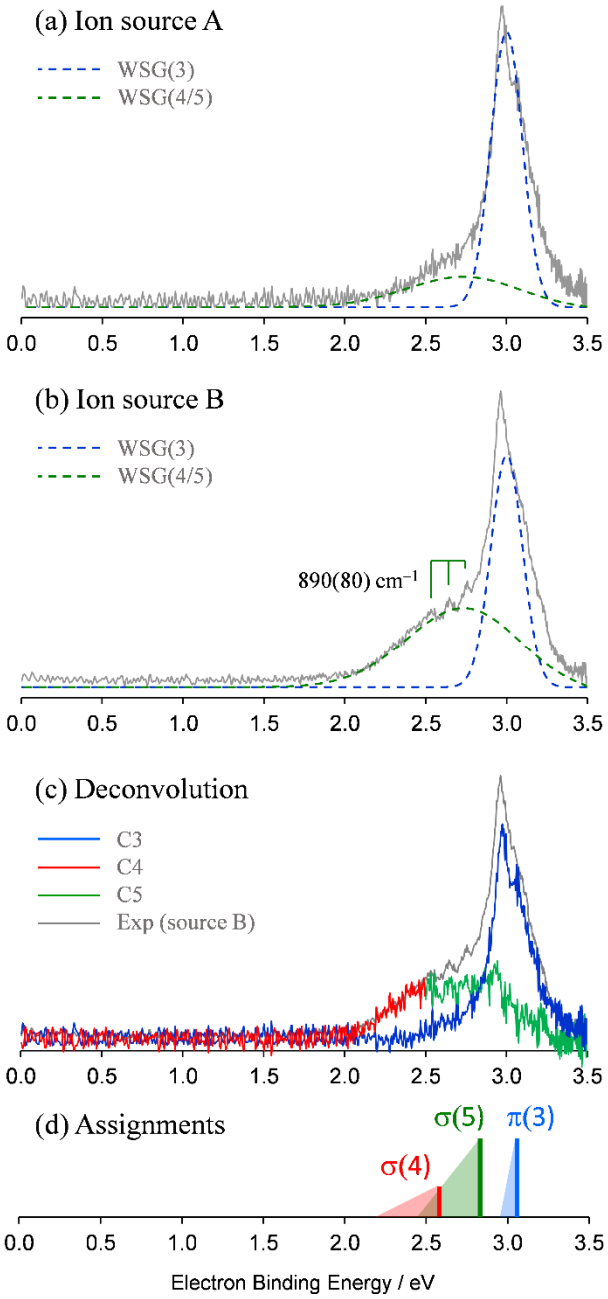

Figure 2. The gray noisy lines in (a), (b), and (c) represent the experimental photoelectron spectra of deprotonated isoxazole collected using ion source conditions A in (a) and B in (b) and (c). The dashed blue and green curves in (a) and (b) represent the Wigner-scaled Gaussian basis functions

WSG(3) and WSG(4/5), respectively, representing the π(3) and σ(4/5) transitions, used to model the experimental spectra. The comb in (b) indicates a vibrational progression, partially resolved in the experimental spectrum, attributed to an in-plane ring-distortion mode of the C5 isomer. (c) Deconvolution of the source B experimental spectrum into the spectra of C4/C5 and C3 isomers. (d) The relevant portion of the triangular-graph spectrum from Figure 1(d), based on the results of the EOM-IP-CCSD/aug-cc-pVTZ calculations for the C5-, C3-, and C4-anion isomers.

Figure 3

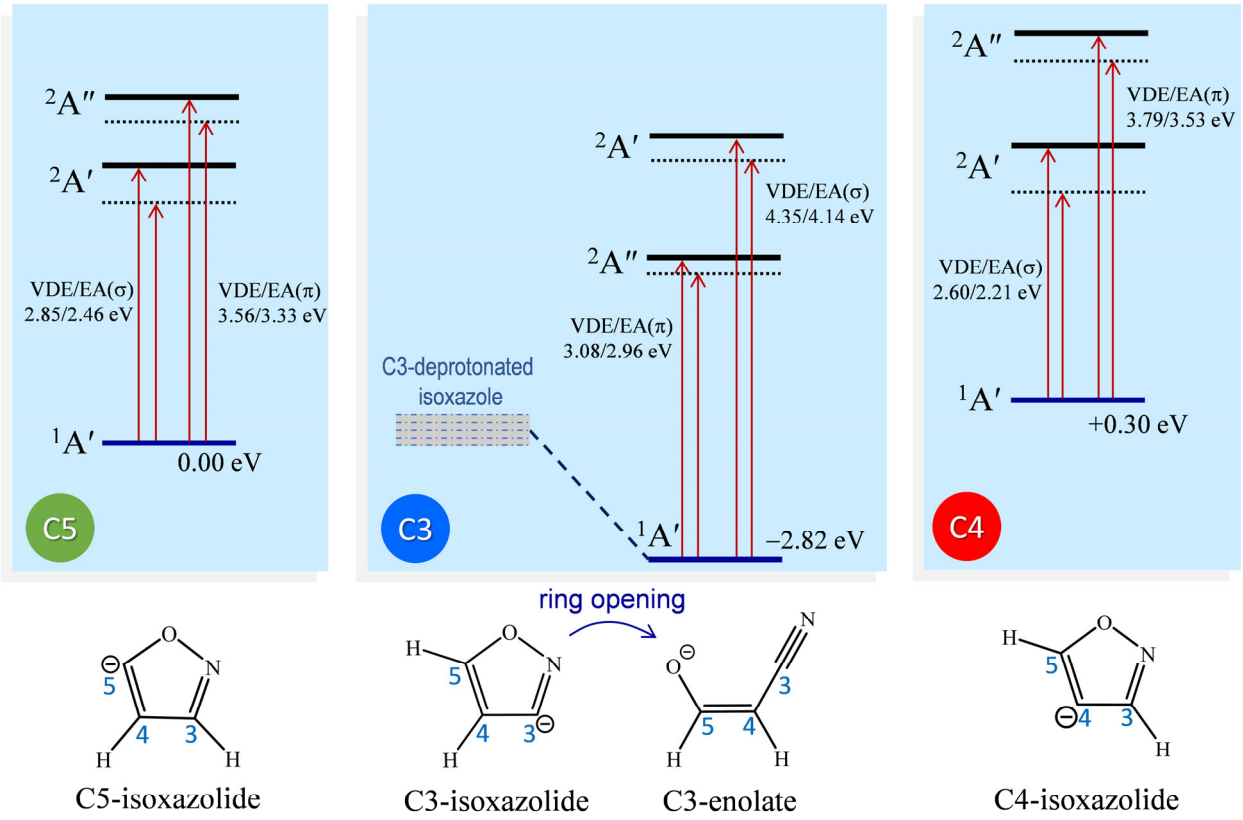

Figure 3. Isomers of the isoxazolide anion formed by the removal of H^+ from isoxazole. All relative energy values are calculated at the CCSD and EOM-IP-CCSD levels of theory with the aug-cc-pVTZ basis set. The dashed energy levels for the neutral (doublet) states correspond to the optimized radical structures, while the solid lines represent the corresponding neutral-state energy levels accessed in vertical photodetachment of the anions.

Figure 4

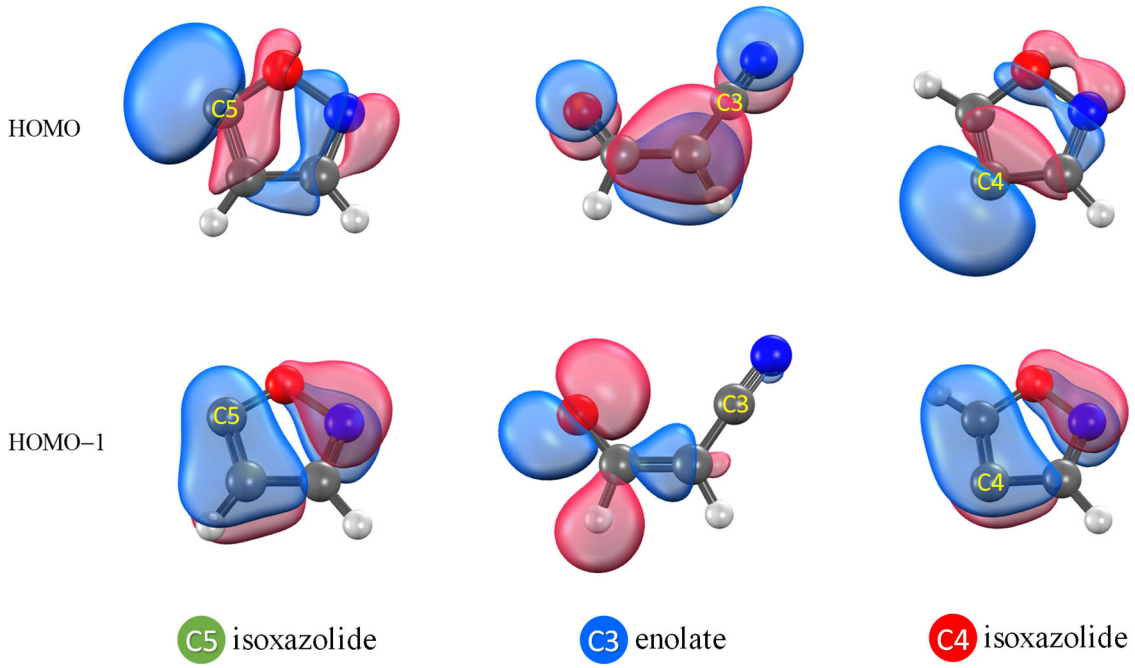

Figure 4. The HOMO (top row) and HOMO-1 (second row) of each of the anion isomers discussed in this work, calculated at the CCSD level of theory with the aug-cc-pVTZ basis set. The surfaces shown correspond to an isovalue of 0.10.

Scheme 1. The structures of oxazole and isoxazole.

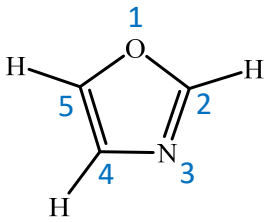

Oxazole

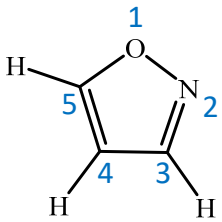

Isoxazole

TOC graphic